CrystEngComm

Accepted Manuscript

CrystEngComm

www.rsc.org/crystengcomm

Volume 18 | Number 1 | 7 January 2016 | Pages 1–184

ROYAL SOCIETY OF CHEMISTRY

HIGHLIGHT
Tiddo J. Mooibroek, Antonio Frontera et al
Towards design strategies for anion–π interactions in crystal engineering

175 YEARS

CrystEngComm

ARTICLE

What a difference a tail makes: 2D→2D parallel interpenetration of sheets to interpenetrated nbo networks using ditopic-4,2':6',4''-terpyridine ligands

Y. Maximilian Klein,[a] Alessandro Prescimone,[a] Markus Neuburger,[a] Edwin C. Constable[a] and Catherine E. Housecroft*[a]

Under conditions of crystal growth by layering at room temperature, 1,4-bis(*n*-hexoxy)-2,5-bis(4,2':6',4''-terpyridin-4'-yl)benzene (**4**) or 1,4-bis(*n*-decoxy)-2,5-bis(4,2':6',4''-terpyridin-4'-yl)benzene (**5**) reacts with $ZnCl_2$ to yield $[Zn_2Cl_4(4)]_n$ or $[Zn_2Cl_4(5)\cdot2MeOH]_n$. The compounds crystallize in the *C*2/*c* space group with 2-dimensional (4,4) nets which interpenetrate in a 2D→2D parallel manner. The ligands act as planar 4-connecting nodes linked through the zinc(II) centres. In contrast, 1,4-bis(3-phenylpropoxy)-2,5-bis(4,2':6',4''-terpyridin-4'-yl)benzene (**6**) reacts with $ZnBr_2$ to give $[Zn_2Br_4(6)\cdot H_2O]_n$ which crystallizes in the trigonal *R*–3 space group with a 3D assembly consisting of 2-fold interpenetrating **nbo** nets. Ligand **6** acts as a 4-connecting node and the zinc(II) centres are linkers. The pendant phenyl rings in **6** lie over the 4,2':6',4''-tpy domains in an adjacent net and the resulting close association of the interpenetrated nets leads to a highly porous network.

Introduction

The design and assembly of coordination architectures incorporating 4,2':6',4''-terpyridine (4,2':6',4''-tpy, Scheme 1) ligands is a mature strategy in crystal engineering.[1,2,3] A 4,2':6',4''-tpy ligand presents a V-shaped building block, coordinating only through the outer N-donors.[1,2] Kröhnke[4] or Wang and Hanan[5] synthetic methodologies permit ready functionalization of the 4'-position of the tpy unit. If the functional group is non-coordinating, the common assembly motifs for architectures supported by 4,2':6',4''-tpy ligands are 1D-chains and 2D-sheets depending upon the coordination geometry of the metal nodes.[1,2] The introduction of coordinatively non-innocent domains such as pyridyl[6] or carboxylate[7] moieties is a proven approach to increasing the dimensionality of 4,2':6',4''-tpy-based coordination assemblies.

Another approach to increasing architectural complexity is the use of ditopic ligands comprising two 4,2':6',4''-tpy domains connected by a spacer (Scheme 1). Ligands in this class are also of interest as optoelectronic materials[8] and for the assembly of supramolecular organic frameworks for CO_2 adsorption.[9] The coordination chemistry of ditopic bis(4,2':6',4''-tpy) and isomeric bis(3,2':6',3''-tpy) ligands remains relatively unexplored. When the spacer (Scheme 1) is a 1,1'-ferrocenyl unit, its preference for a *cisoid*-conformation leads to the

bis(4,2':6',4''-tpy) ligand adopting a folded conformation and reaction with $ZnCl_2$ produces a double-stranded 1D-coordination polymer.[10] With the exception of this example, ditopic bis(4,2':6',4''-tpy) ligands typically contain a 1,4-C_6H_4 spacer which predisposes the ligand towards functioning as a 4-connecting node, either as a planar or approximately tetrahedral node (Scheme 2). Additional structural variation may be achieved through a different substitution pattern in the aryl spacer,[11] or by replacing the 4,2':6',4''-tpy by 3,2':6',3''-tpy metal-binding units.[12] We are currently exploring a series of ditopic bis(4,2':6',4''-tpy) and bis(3,2':6',3''-tpy) ligands with different alkoxy substituents attached to the central spacer. We have shown that reaction of **1** (Scheme 3) with Co(NCS)$_2$ leads to a 3D {$4^2 \cdot 8^4$} **lvt** net.[12] This assembly depends upon both the metal and ligand acting as 4-connecting nodes (planar and approximately tetrahedral, respectively). In contrast, combining **2** (Scheme 3) with $ZnCl_2$ or $ZnBr_2$ leads to 2D-sheets in which the ligands are the unique nodes.[13,14] While the (4,4) nets in $[\{Zn_2Cl_4(2)\}\cdot4H_2O]_n$ and $[\{Zn_2Br_4(2)\}]_n$ interpenetrate in a 2D→2D parallel fashion, analogous nets present in $[\{Zn_2Br_4(3)\}\cdot2C_6H_4Cl_2]_n$ and $[\{Zn_2I_4(3)\}\cdot2.3C_6H_4Cl_2]_n$ show no interpenetration.[14] The *n*octyl-chains in **2** are in extended conformations in $[\{Zn_2Cl_4(2)\}\cdot4H_2O]_n$ and $[\{Zn_2Br_4(2)\}]_n$, and are threaded within the interpenetrated sheets. We have previously suggested that the long chains may assist in directing the assembly process.[13] We have now extended the

CrystEngComm Accepted Manuscript

ARTICLE

investigation to ligands **4–6**. Ligands **4** and **5** possess shorter and longer alkoxy tails than **3**, while each alkoxy chain in **6** is terminated by a phenyl group.
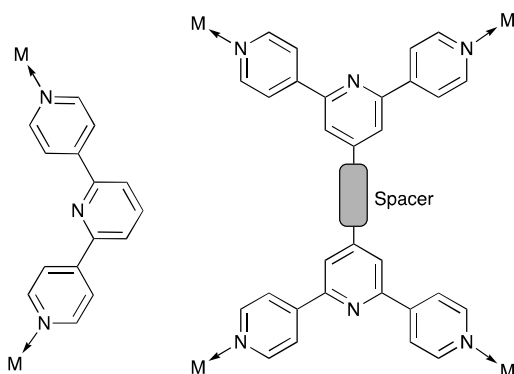
Scheme 1. Typical divergent coordination modes of 4,2':6',4''-tpy units in mono- and ditopic ligands.

Planar 4-connecting   ≈Tetrahedral 4-connecting
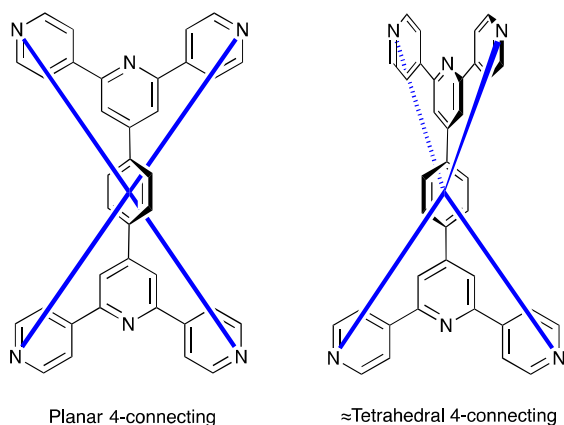
Scheme 2. Ditopic bis(4,2':6',4''-tpy) ligands as limiting planar and tetrahedral 4-connecting nodes.

1   R = ^{n}octyl

2 R = ^{n}octyl
3 R = Me
4 R = ^{n}hexyl
5 R = ^{n}decyl
6 R = CH$_2$CH$_2$CH$_2$Ph
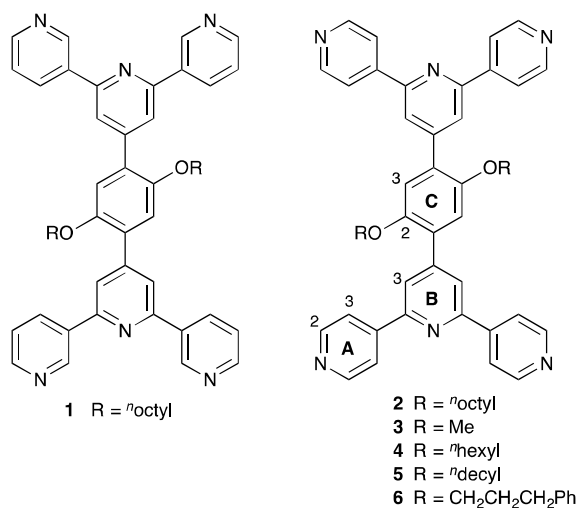
Scheme 3. Structures of ligands **1–6**. Ring labelling is used for NMR assignments; in compound **6**, the phenyl ring is ring D. Alkoxy chains are labelled C/H$^{a, b ...}$ starting at the OCH$_2$ group.

Experimental

General. ^{1}H and ^{13}C NMR spectra were recorded on a Bruker DRX-500 NMR spectrometer with chemical shifts referenced to residual solvent peaks (TMS = δ 0 ppm). Electrospray ionisation (ESI) mass spectra were measured on a Bruker esquire 3000plus spectrometer or Shimadzu LCMS-2020 instrument, and high resolution ESI mass spectra on a Bruker maXis 4G QTOF instrument. For GC/MS analysis, a Shimadzu GCMS/QP2010 SE gas chromatograph system with ZB-5HT inferno column (30 m × 0.25 mm × 0.25 mm), at 1 mL/min He-Flow rate (split = 20:1) with a Shimadzu mass detector (EI 70 eV) was used.

1-Bromohexane, 1-bromodecane, 2,5-dibromohydroquinone and 1-bromo-3-phenylpropane were purchased from Sigma-Aldrich. 1,4-Dibromo-2,5-bis(^{n}hexoxy)benzene (**4a**) and 1,4-dibromo-2,5-bis(^{n}decoxy)benzene (**5a**) have previously been reported[15] but we find the following method of synthesis convenient, giving a higher yield of **4a**.

Compound 4a. 2,5-Dibromohydroquinone (2.00 g, 7.47 mmol), 1-bromohexane (2.64 mL, 3.11 g, 18.7 mmol) and anhydrous K$_2$CO$_3$ (3.10 g, 22.4 mmol) were added to dry DMF (100 mL) and the mixture was heated at 100 °C for ~15 h. The reaction mixture was cooled to room temperature, then transferred to a beaker containing 100 mL of ice water and stirred for 30 min. The precipitate was filtered, washed with water (3 × 30 mL) and dried *in vacuo*. The product was recrystallized from a mixture of EtOH and CHCl$_3$ and isolated as white crystals (3.05 g, 6.99 mmol, 93.6%). NMR spectroscopic data agreed with the literature.[15] GC-EI-MS *m/z* 436.1 [M]$^{+}$ (calc. 436.0). M.p. = 64.4 °C, deviating from the literature value of 51.3-53.1 °C.[15]

Compound 5a. The method was as for **4a** starting with 2,5-dibromohydroquinone (1.00 g, 3.73 mmol), 1-bromodecane (2.33 mL, 2.48 g, 11.2 mmol) and anhydrous K$_2$CO$_3$ (1.55 g, 11.2 mmol). **5a** was isolated as white crystals (1.83 g, 3.34 mmol, 89.5%). M.p. = 74.4 °C. ^{1}H NMR spectroscopic data agreed with the literature.[15] ^{13}C{^{1}H} NMR (126 MHz, CDCl$_3$) δ / ppm 150.2 (C^{C2}), 118.6 (C^{C3}), 111.3 (C^{C1}), 70.5 (C^{a}), 32.1 (C^{CH2}), 29.7 (C^{CH2}), 29.65 (C^{CH2}), 29.45 (C^{CH2}), 29.5 (C^{CH2}), 29.3 (C^{b}), 26.1 (C^{c}), 22.8 (C^{CH2}), 14.3 (C^{j}). GC-EI-MS *m/z* 548.3 [M]$^{+}$ (calc. 548.2).

Compound 6a. 2,5-Dibromohydroquinone (1.00 g, 3.73 mmol), 1-bromo-3-phenylpropane (1.42 mL, 1.86 g, 9.33 mmol) and anhydrous K$_2$CO$_3$ (1.55 g, 11.2 mmol) were added to dry DMF (100 mL) and the mixture was heated at 100 °C for ~15 h. The reaction mixture was cooled to room temperature, then transferred to a beaker containing 100 mL of ice water, stirred for 30 min and extracted with CH$_2$Cl$_2$ (200 mL). The organic phase was dried over MgSO$_4$ and concentrated *in vacuo*. The product was recrystallized from a mixture of EtOH and CHCl$_3$ and isolated as white crystals (1.68 g, 3.33 mmol, 89.3 %). M.p. = 88.8 °C. ^{1}H NMR (500 MHz, CDCl$_3$) δ / ppm 7.30 (m, 4H, H^{D3}), 7.24–7.17 (m, 6H, H^{D2+D4}), 7.06 (s, 2H, H^{C3}), 3.95 (t, *J* = 6.2 Hz, 4H, H^{a}), 2.86 (m, 4H, H^{c}), 2.11 (m, 4H, H^{b}). ^{13}C{^{1}H} NMR (126 MHz, CDCl$_3$) δ / ppm 150.1

Page 3 of 12

CrystEngComm

Journal Name

View Article Online
DOI: 10.1039/C7CE00686A

ARTICLE

(C^{C2}), 141.4 (C^{D1}), 128.7 ($C^{D2/D3/D4}$), 128.6 ($C^{D2/D3/D4}$), 126.1 ($C^{D2/D3/D4}$), 118.6 (C^{C3}), 111.3 (C^{C1}), 69.1 (C^a), 32.1 (C^c), 30.9 (C^b). GC-EI-MS m/z 503.8 [M]$^+$ (calc. 504.0).

Compound 4b. Compound **4a** (1.80 g, 4.13 mmol) and dry Et$_2$O (150 mL) were added to a dried flask and cooled to 0 °C in an ice bath. ^{n}Butyllithium (1.6 M in hexanes, 7.74 mL, 12.4 mmol) was added slowly to the Et$_2$O solution over a period of 20 min and the temperature maintained at 0 °C for 6h. Dry DMF (0.96 mL, 12.4 mmol) was added and the solution was stirred for ~15 h, during which time it was allowed to warm to room temperature. The reaction mixture was neutralized with saturated aqueous NH$_4$Cl and extracted with CH$_2$Cl$_2$ (200 mL). The organic phase was dried over MgSO$_4$ and concentrated *in vacuo*. **4b** was isolated as a yellow solid (0.85 g, 2.54 mmol, 61.5%) and used without further purification. M.p. = 68.6 °C. The ^{1}H NMR spectrum agreed with literature data.[16] ^{13}C{^{1}H} NMR (126 MHz, CDCl$_3$) δ / ppm 189.6 (C^{CHO}), 155.4 (C^{C2}), 129.4 (C^{C1}), 111.8 (C^{C3}), 69.38 (C^a), 31.6 ($C^{d/e}$), 29.2 (C^b), 25.8 (C^c), 22.7 ($C^{d/e}$), 14.1 (C^f). GC-EI-MS m/z 334.2 [M]$^+$ (calc. 334.2).

Compound 5b. The method and volumes of solvents were as for the synthesis of **4b**, but using **5a** (3.0 g, 5.47 mmol), ^{n}BuLi (1.6 M in hexanes, 10.3 mL, 16.4 mmol), dry DMF (1.27 mL, 16.4 mmol). **5b** was obtained as a yellow solid (2.27 g, 5.08 mmol, 92.9%) and used without further purification. M.p. = 80.3 °C. ^{1}H NMR (500 MHz, CDCl$_3$) δ / ppm 10.52 (s, 2H, H^{CHO}), 7.43 (s, 2H, H^{C3}), 4.08 (t, J = 6.5 Hz, 4H, H^a), 1.82 (m, 4H, H^b), 1.46 (m, 4H, H^c), 1.40–1.18 (m, 24H, H^{d-i}), 0.87 (m, 6H, H^j). ^{13}C{^{1}H} NMR (126 MHz, CDCl$_3$) δ / ppm 189.6 (C^{CHO}), 155.4 (C^{C2}), 129.4 (C^{C1}), 111.8 (C^{C3}), 69.4 (C^a), 32.0 (C^{CH2}), 29.7 (C^{CH2}), 29.68 (C^{CH2}), 29.46 (C^{CH2}), 29.45 (C^{CH2}), 29.2 (C^b), 26.15 (C^c), 22.8 (C^{CH2}), 14.3 (C^j). GC-EI-MS m/z 446.4 [M]$^+$ (calc. 446.3).

Compound 6b. The method and volumes of solvents were as for the synthesis of **4b**, but using **6a** (1.5 g, 2.97 mmol), ^{n}BuLi (1.6 M in hexanes, 5.57 mL, 8.91 mmol) and dry DMF (0.69 mL, 8.91 mmol). **6b** was isolated as a yellow solid (1.08 g, 2.68 mmol, 90.3%) and used without further purification. M.p. = 102.6 °C. ^{1}H NMR (500 MHz, CDCl$_3$) δ / ppm 10.47 (s, 2H, H^{CHO}, 7.41 (s, 2H, H^{C3}), 7.30 (m, 4H, H^{D3}), 7.24–7.19 (m, 6H, H^{D2+D4}), 4.11 (t, J = 6.2 Hz, 4H, H^a), 2.83 (t, J = 7.6 Hz, 4H, H^c), 2.19 (m, 4H, H^b). ^{13}C{^{1}H} NMR (126 MHz, CDCl$_3$) δ / ppm 189.4 (C^{CHO}), 155.2 (C^{C2}), 141.10 (C^{D1}), 129.36 (C^{C1}), 128.67 ($C^{D2/D3/D4}$), 128.53 ($C^{D2/D3/D4}$), 126.27 ($C^{D2/D3/D4}$), 111.8 (C^{C3}), 68.3 (C^a), 32.4 (C^c), 30.7 (C^b). GC-EI-MS m/z 402.0 (calc. 402.2).

Compound 4. Compound **4b** (0.3 g, 0.9 mmol) was dissolved in EtOH (100 mL), then 4-acetylpyridine (0.41 mL, 0.44 g, 3.59 mmol) and crushed solid KOH (0.20 g, 3.59 mmol) were added. Aqueous NH$_3$ (32%, 3.0 mL) was added dropwise and the reaction mixture was stirred at room temperature for ~15 h. The precipitate was collected by filtration and washed with water, EtOH and Et$_2$O (3 × 10 mL, each). Compound **4** was obtained as a white solid (0.15 g, 0.21 mmol, 23.3%). Decomp > 280 °C. ^{1}H NMR (500 MHz, CDCl$_3$) δ / ppm 8.80 (m, 8H, H^{A2}), 8.11 (s, 4H, H^{B3}), 8.09 (m, 8H, H^{A3}), 7.16 (s, 2H, H^{C2}), 4.06 (t, J = 6.3

Hz, 4H, H^a), 1.74 (m, 4H, H^b), 1.37 (m, 4H, H^c), 1.25–1.09 (m, 8H, H^{d+e}), 0.76 (t, J = 7.1 Hz, 6H, H^f). ^{13}C{^{1}H} NMR (126 MHz, CDCl$_3$) δ / ppm 154.8 (C^{B2}), 150.7 (C^{A2+C3}), 148.3 (C^{B4}), 146.2 (C^{A4}), 129.3 (C^{C1}), 121.6 (C^{B3}), 121.3 (C^{A3}), 115.3 (C^{C2}), 69.9 (C^a), 31.6 ($C^{d/e}$), 29.5 (C^b), 26.1 (C^c), 22.6 ($C^{d/e}$), 14.1 (C^f). ESI-MS m/z 741.6 [M+H]$^+$ (calc. 741.4). HR ESI-MS m/z 371.1998 [M+2H]$^{2+}$ (calc. 371.1992).

Compound 5. The method and volumes of solvent were as for the synthesis of **4**, but starting with **5b** (0.60 g, 1.34 mmol, 4-acetylpyridine (0.61 mL, 0.66 g, 5.36 mmol), KOH (0.3 g, 5.36 mmol) and aqueous NH$_3$ (32%, 3.42 mL). Compound **5** was obtained as a white solid (0.25 g, 0.3 mmol, 22.1%). M.p. = 239.8 °C. ^{1}H NMR (500 MHz, CDCl$_3$) δ / ppm 8.81 (m, 8H, H^{A2}), 8.11 (s, 4H, H^{B3}), 8.09 (m, 8H, H^{A3}), 7.16 (s, 2H, H^{C2}), 4.06 (t, J = 6.2 Hz, 4H, H^a), 1.74 (m, 4H, H^b), 1.37 (m, 4H, H^c), 1.23 (m, 8H, H^i), 1.19–1.08 (m, 18H, H^{d-h}), 0.84 (t, J = 7.2 Hz, 6H, H^j). ^{13}C{^{1}H} NMR (126 MHz, CDCl$_3$) δ / ppm 154.8 (C^{B2}), 150.8 (C^{C3}), 150.7 (C^{A2}), 148.3 (C^{B4}), 146.2 (C^{A4}), 129.3 (C^{C1}), 121.5 (C^{B3}), 121.3 (C^{A3}), 115.4 (C^{C2}), 69.9 (C^a), 32.0 (C^{CH2}), 29.65 (C^{CH2}), 29.6 (C^{CH2}), 29.5 (C^{CH2}), 29.4 (C^{CH2}), 26.5 (C^c), 22.8 (C^{CH2}), 14.2 (C^j). ESI-MS m/z 853.7 [M+H]$^+$ (calc. 853.5). HR ESI-MS m/z 427.2625 [M+2H]$^{2+}$ (calc. 427.2618).

Compound 6. The method and solvent volumes were as for **4** but starting with **6b** (0.89 g, 2.21 mmol), 4-acetylpyridine (1.13 mL, 1.23 g, 9.95 mmol, KOH (0.56 g, 9.95 mmol) and aqueous NH$_3$ (32%, 17 mL). Compound **6** was obtained as a pale yellow solid (0.74 g, 0.92 mmol, 41.4%). Decomp. > 260°C. ^{1}H NMR (500 MHz, CDCl$_3$) δ / ppm 8.80 (m, 8H, H^{A2}), 8.12 (s, 4H, H^{B3}), 8.09 (m, 8H, H^{A3}), 7.19–7.10 (m, 8H, H$^{C2/D3+D4}$), 6.98 (m, 4H, H^{D2}), 4.09 (t, J = 6.1 Hz, 4H, H^a), 2.69 (m, 4H, H^c), 2.09 (m, 4H, H^b). ^{13}C{^{1}H} NMR (126 MHz, CDCl$_3$) δ / ppm 154.9 (C^{B2}), 150.8 (C^{A2}), 150.6 (C^{C3}), 148.3 (C^{B4}), 146.2 (C^{A4}), 140.9 (C^{D1}), 129.4 (C^{C1}), 128.6 ($C^{C2/D3/D4}$), 128.3 (C^{D2}), 126.3 ($C^{C2/D3/D4}$), 121.5 (C^{B3}), 121.3 (C^{A3}), 115.5 ($C^{C2/D3/D4}$), 68.9 (C^a), 32.4 (C^c), 31.1 (C^b). ESI-MS m/z 809.6 [M+H]$^+$ (calc. 809.4). HR ESI-MS m/z 809.3587 [M+H]$^+$ (calc. 809.3599).

[Zn$_2$Cl$_4$(4)]$_n$. A MeOH (8 mL) solution of ZnCl$_2$ (1.36 mg, 0.01 mmol) was layered over a CHCl$_3$ (5 mL) solution of **4** (7.41 mg, 0.01 mmol) and the crystallization tube was left to stand at room temperature. Yellow crystals of [Zn$_2$Cl$_4$(**4**)]$_n$ (7.8 mg) were obtained after 1-2 weeks. Satisfactory elemental analysis of the bulk sample could not be obtained; see text for discussion of powder diffraction data.

[Zn$_2$Cl$_4$(5)·2MeOH]$_n$. A MeOH (8 mL) solution of ZnCl$_2$ (2.04mg, 0.015 mmol) was layered over a CHCl$_3$ (5 mL) solution of **5** (12.8 mg, 0.015 mmol) and the crystallization tube was left to stand at room temperature. Pale yellow crystals of [Zn$_2$Cl$_4$(**5**)]$_n$ (3.2 mg) were obtained after 1-2 weeks. Satisfactory elemental analysis of the bulk sample could not be obtained; see Fig. S1† for powder diffraction data.

[Zn$_2$Br$_4$(6)·H$_2$O]$_n$. A MeOH (8 mL) solution of ZnBr$_2$ (4.5 mg, 0.02 mmol) was layered over a CHCl$_3$ (5 mL) solution of **6** (16.2 mg, 0.02 mmol) and the crystallization tube was left to stand at room temperature. Yellow crystals of [{Zn$_2$Br$_4$(**6**)}·H$_2$O]$_n$ (6.7 mg) were obtained after 1-2 weeks.

Satisfactory elemental analysis of the bulk sample could not be obtained; see text for discussion of powder diffraction data.

Crystallography. Single crystal data were collected on a STOE StadiVari diffractometer equipped with a Pilatus300K detector and with a Metaljet D2 source or a Bruker APEX-II diffractometer; data reduction, solution and refinement used the programs STOE X-AREA, STOE X-RED, APEX2, SuperFlip and CRYSTALS respectively.[17,18,19] SQUEEZE[20] was used in $[Zn_2Cl_4(4)]_n$ because solvent molecules could not be identified in the residual electron density. Four cavities of ~350 Å^3 were identified, and in each, contributions corresponding to 68 electrons were removed, equating to 3 to 4 molecules of MeOH per cavity. SQUEEZE was used in the solvent region of $[Zn_2Br_4(6)\cdot H_2O]_n$. There are 20587 Å^3 out of 28228 Å^3 accessible to solvent molecules,[20] which, according to SQUEEZE corresponds to 646 electrons or 4 molecules of MeOH per formula unit. Unfortunately the refinement did not improve after applying SQUEEZE, therefore the structure was left at this stage of refinement without unambiguously identifying solvent molecules in the residual electron density; it follows that the calculated density is low. Powder diffraction data were collected on a Stoe Stadi P powder diffractometer. Structure analysis used the program Mercury v. 3.7[21,22] and TOPOS.[23]

$[Zn_2Cl_4(4)]_n$. $C_{48}H_{48}Cl_4N_6O_2Zn_2$, M = 1013.52, yellow block, monoclinic, space group $C2/c$, a = 20.4985(9), b = 11.6491(3), c = 23.7457(10) Å, β = 91.737(4)^o, U = 5667.6(4) Å^3, Z = 4, D_c = 1.188 Mg m^{-3}, μ(Ga-Kα) = 2.036 mm^{-1}, T = 123 K. Total 95099 reflections, 5516 unique, R_{int} = 0.057. Refinement of 3189 reflections (280 parameters) with $I > 2\sigma$ (I) converged at final $R1$ = 0.0451 ($R1$ all data = 0.0676), $wR2$ = 0.0510 ($wR2$ all data = 0.0578), gof = 0.8726. CCDC 1541160.

$[Zn_2Cl_4(5)\cdot 2MeOH]_n$. $C_{58}H_{72}Cl_4N_6O_4Zn_2$, M = 1189.82, colourless plate, monoclinic, space group $C2/c$, a = 20.777(2), b = 11.6382(9), c = 23.8738(17) Å, β = 90.074(7)^o, U = 5772.8(8) Å^3, Z = 4, D_c = 1.369 Mg m^{-3}, μ(Cu-Kα) = 3.122 mm^{-1}, T = 123 K. Total 34161 reflections, 5360 unique, R_{int} = 0.034. Refinement of 5077 reflections (332 parameters) with $I > 2\sigma$ (I) converged at final $R1$ = 0.0726 ($R1$ all data = 0.0749), $wR2$ = 0.1722 ($wR2$ all data = 0.1726), gof = 0.7625. CCDC 1541161.

$[Zn_2Br_4(6)\cdot H_2O]_n$. $C_{54}H_{44}Br_4N_6O_3Zn_2$, M = 1275.36, yellow block, trigonal, space group $R–3$, a = b = 35.9593(6), c = 25.1227(3) Å, U = 28133.2(9) Å^3, Z = 9, D_c = 0.677 Mg m^{-3}, μ(Ga-Kα) = 1.410 mm^{-1}, T = 123 K. Total 140567 reflections, 12851 unique, R_{int} = 0.073. Refinement of 6571 reflections (316 parameters) with $I > 2\sigma$ (I) converged at final $R1$ = 0.0898 ($R1$ all data = 0.1242), $wR2$ = 0.0719 ($wR2$ all data = 0.0924), gof = 0.9393. CCDC 1541159.

Results and discussion

Ligand synthesis and characterization

Compounds **4**, **5** and **6** were prepared as summarized in Scheme 4. The dibromo-precursors **4a** and **5a** have been previously prepared by bromination of the respective 1,4-dialkoxybenzenes, the latter first being prepared from hydroquinone.[15] However, we found it more convenient to start with the commercially available 2,5-dibromohydroquinone. Reaction of **4a**, **5a** or **6a** with ^{n}BuLi followed by DMF (see Scheme 4) yielded dialdehydes **4b**, **5b** or **6b**. The intermediates were characterized by NMR spectroscopy (assigned using 2D methods) and GC-EI mass spectrometry, before being converted to the bis(4,2':6',4"-tpy) ligands **4–6** using a one-pot Hanan-type[5] synthesis. ^{1}H and ^{13}C NMR spectra were assigned using COSY, HMQC, HMBC and NOESY methods. The ^{1}H NMR spectrum of **5** is shown in Fig. S2†. The disappearance of the ^{1}H NMR resonance at ~ δ 10.5 ppm on going from **4b** to **4**, **5b** to **5**, or **6b** to **6** was consistent with functionalization of the aryl core at both aldehyde sites. The ^{1}H NMR signature of each 4,2':6',4"-tpy unit consisted of a singlet (δ 8.11, 8.11 or 8.12 ppm in **4**, **5** or **6**) for proton H^{B3} and multiplets for protons H^{A2} and H^{A3} at δ 8.80 or 8.81 and 8.09 ppm, respectively (see Scheme 3 for atom labelling). A comparison of the aromatic regions of the ^{1}H NMR spectra of **4, 5**, and **6** is shown in Fig. S3–S5†. The parent ions in the electrospray mass spectra (EIS MS) and high resolution EIS MS of **4–6** (see Experimental section) were in accordance with expected molecular masses.
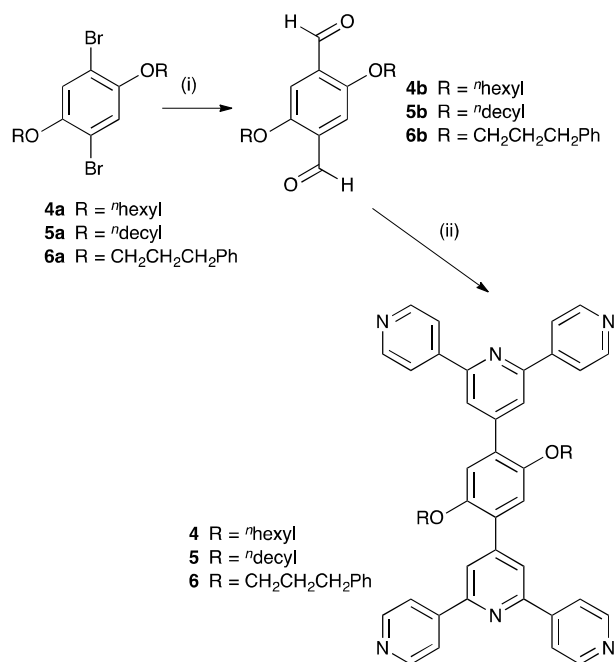
Scheme 4. Synthetic method for preparation of ligands **4**, **5** and **6**. Conditions: (i) ^{n}BuLi, Et$_2$O, 0°C, 6h; DMF, room temperature; (ii) 4-acetylpyridine, KOH, EtOH; aqueous NH$_3$.

Alkoxy chains: 2D→2D parallel interpenetrated sheets

We initially chose to investigate the reactions of ligands **4** and **5** with zinc(II) chloride as an extension of our previous studies of

the 2D networks formed when **2** (*n*octyl functionality) and **3** (methyl functionality) react with ZnX_2 (X = Cl, Br, I). The difference between **4** and **5** is the length of the alkoxy chain (Scheme 3), the *n*hexoxy and *n*decoxy chains in **4** and **5** being, respectively, shorter and longer than the *n*octyl chains known to give 2D→2D parallel interpenetrated sheets in $[\{Zn_2Cl_4(\mathbf{2})\}\cdot 4H_2O]_n$ and $[\{Zn_2Br_4(\mathbf{2})\}]_n$.[13,14] Ligand **4** contains alkoxy chains that are longer than the methyl substituents in $[\{Zn_2Br_4(\mathbf{3})\}\cdot 2C_6H_4Cl_2]_n$ and $[\{Zn_2I_4(\mathbf{3})\}\cdot 2.3C_6H_4Cl_2]_n$; these assemble into 2D-networks with no interpenetration.
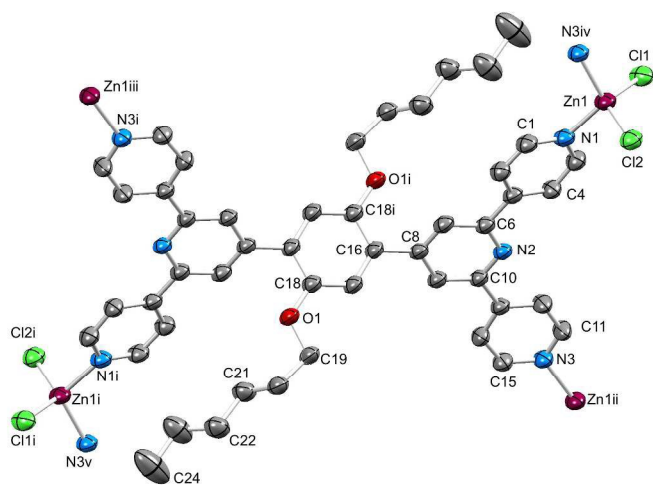
Fig. 1. The repeat unit (with symmetry generated atoms) in $[Zn_2Cl_4(\mathbf{4})]_n$ (H atoms omitted; ellipsoids plotted at 40% probability level). Symmetry codes: i = 1–*x*, –*y*, –*z*; ii = *x*, 1–*y*, $-^1/_2$+*z*; iii = 1–*x*, 1+*y*, $^1/_2$–*z*; iv = *x*, 1–*y*, $^1/_2$+*z*; v = 1–*x*, –1+*y*, $-^1/_2$–*z*. Selected bond parameters: Zn1–N1 = 2.026(3), Zn1–N3^{iv} = 2.034(3), Zn1–Cl1 = 2.2137(11), Zn1–Cl2 = 2.2445(12), O1–C18 = 1.361(4), O1–C19 = 1.439(4) Å; N3^{iv}–Zn1–Cl1 = 107.06(9), N3^{iv}–Zn1–Cl2 = 106.02(10), Cl1–Zn1–Cl2 = 123.64(5), N3^{iv}–Zn1–N1 = 112.07(12), Cl1–Zn1–N1 = 104.68(9), Cl2–Zn1–N1 = 103.35(9), C18–O1–C19 = 118.8(3)°.

A MeOH solution of $ZnCl_2$ was layered over a $CHCl_3$ solution of **4** or **5** and after one to two weeks, X-ray quality crystals were harvested. Single crystal X-ray diffraction revealed the formation of $[Zn_2Cl_4(\mathbf{4})]_n$ and $[Zn_2Cl_4(\mathbf{5})\cdot 2MeOH]_n$. The lattice in $[Zn_2Cl_4(\mathbf{4})]_n$ also contains solvent molecules, but these were not unambiguously identified (see Experimental section). Both $[Zn_2Cl_4(\mathbf{4})]_n$ and $[Zn_2Cl_4(\mathbf{5})\cdot 2MeOH]_n$ crystallize in the monoclinic space group *C*2/*c*, with similar cell dimensions. These parameters are also comparable with those of $[\{Zn_2Cl_4(\mathbf{2})\}\cdot 4H_2O]_n$ and $[\{Zn_2Br_4(\mathbf{2})\}]_n$ (Table S1†),[13,14] consistent with the assembly of similar extended structures. The asymmetric unit in each of $[Zn_2Cl_4(\mathbf{4})]_n$ and $[Zn_2Cl_4(\mathbf{5})\cdot 2MeOH]_n$ contains one $ZnCl_2$ unit and half of ligand **4** or **5**; the second half of the repeat unit is generated by inversion. The repeat units of $[Zn_2Cl_4(\mathbf{4})]_n$ and $[Zn_2Cl_4(\mathbf{5})\cdot 2MeOH]_n$ with symmetry generated atoms are shown in Figs. 1 and S6†, and selected bond lengths and angles are given in the figure captions. As expected,[1] each of ligands **4** and **5** coordinates through only the four outer nitrogen atoms. Atom Zn1 (in both structures) is tetrahedrally sited, bound to

two Cl atoms and to two N atoms of different ligands. The angles that define the tetrahedral coordination sphere are in the range 103.35(9) to 123.64(5)° in $[Zn_2Cl_4(\mathbf{4})]_n$, and 104.44(10) to 122.26(5)° in $[Zn_2Cl_4(\mathbf{5})\cdot 2MeOH]_n$. The 4,2':6',4"-tpy unit in each compound deviates from planarity to a similar degree; in $[Zn_2Cl_4(\mathbf{4})]_n$, the angles between the planes of adjacent pyridine rings are 0.3 and 15.9°, and the corresponding angles in $[Zn_2Cl_4(\mathbf{5})\cdot 2MeOH]_n$ are 3.5 and 16.4°. The twist of the arene spacer with respect to the pyridine ring to which it is bonded is 51.5° for coordinated **4** and 51.8° for **5**.

Ligand **4** acts as a 4-connecting node, generating a uninodal (4,4) net with the zinc(II) centres functioning only as linkers. Fig. 2a illustrates that each metallomacrocycle in the net is defined by two 4,2':6',4"-tpy domains from different ligands (coloured orange in Fig. 2a) and two 'half-ligands' (shown in blue in Fig. 2a). The non-planarity of the macrocyclic units leads to a net with a corrugated topology. The (4,4) nets lie in the *bc*-plane and Fig. 2b views part of one net looking down the *c*-axis. The centroids of the arene rings running across the middle of Fig. 2b correspond to the nodes of the net. The *n*hexoxy chains adopt an extended conformation and are directed within the corrugated sheet. These structural features are replicated in $[Zn_2Cl_4(\mathbf{5})\cdot 2MeOH]_n$ (Fig. 2c). The profile (Fig. 2b and 2c) of the (4,4) nets in $[Zn_2Cl_4(\mathbf{4})]_n$ and $[Zn_2Cl_4(\mathbf{5})\cdot 2MeOH]_n$ are essentially invariant of the length of the alkoxy tail with the node...node separations being 16.6 and 16.7 Å, respectively; the distance is measured between centroids of the arene rings. The corresponding separations in $[\{Zn_2Cl_4(\mathbf{2})\}\cdot 4H_2O]_n$ and $[\{Zn_2Br_4(\mathbf{2})\}]_n$ which contain *n*octyl chains[13,14] are 16.6 and 16.8 Å, respectively. The corrugated topology of the (4,4) nets in $[Zn_2Cl_4(\mathbf{4})]_n$ and $[Zn_2Cl_4(\mathbf{5})\cdot 2MeOH]_n$ allows them to interpenetrate in a 2D→2D parallel manner, just as we have previously observed in $[\{Zn_2Cl_4(\mathbf{2})\}\cdot 4H_2O]_n$ and $[\{Zn_2Br_4(\mathbf{2})\}]_n$.[13,14] This is shown for $[Zn_2Cl_4(\mathbf{4})]_n$ in Fig. 3. We have previously shown that shortening the tails (i.e. going from *n*octoxy to methoxy functionalization) causes the profile of the corrugated sheet to change.[14] Although a (4,4) net is retained, the profile flattens, switching off the 2D→2D parallel interpenetration. The persistence of the same structural motifs in the series of compounds $[Zn_2Cl_4(\mathbf{4})]_n$, $[\{Zn_2Cl_4(\mathbf{2})\}\cdot 4H_2O]_n$, $[\{Zn_2Br_4(\mathbf{2})\}]_n$ and $[Zn_2Cl_4(\mathbf{5})\cdot 2MeOH]_n$ further supports our earlier proposal that the chain contributes to the assembly process. The structures do not feature close alignment of the chains, indicating that inter-chain van der Waals interactions are not a contributing factor. In each of $[Zn_2Cl_4(\mathbf{4})]_n$ and $[Zn_2Cl_4(\mathbf{5})\cdot 2MeOH]_n$, the alkoxy chain lies over two pyridine rings of a 4,2':6',4"-tpy unit (Fig. 4), giving rise to short CH...π contacts.[24] The closest CH...c□□□□□□□distances are 3.01 in $[Zn_2Cl_4(\mathbf{4})]_n$ and 3.47 Å in $[Zn_2Cl_4(\mathbf{5})\cdot 2MeOH]_n$. We note that a similar arrangement is observed in $[\{Zn_2Cl_4(\mathbf{2})\}\cdot 4H_2O]_n$ (CSD[25] refcode NOTPUJ)[13] with the closest CH...π contact being 2.95 Å (Fig. S7†).
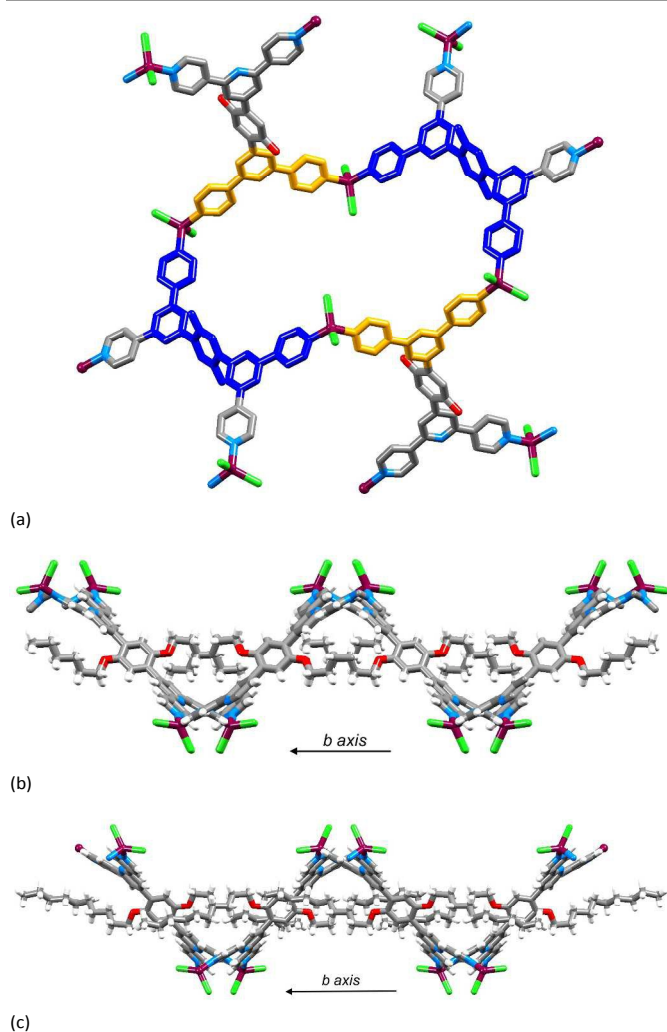
Fig. 2. (a) One macrocyclic unit within one network in $[Zn_2Cl_4(\mathbf{4})]_n$ contains four Zn atoms, two complete 4,2':6',4''-tpy domains (orange) and two 'half-ligands' (blue). ^{n}Hexoxy chains and H atoms are omitted for clarity. Part of one net in (b) $[Zn_2Cl_4(\mathbf{4})]_n$ and (c) $[Zn_2Cl_4(\mathbf{5})\cdot 2MeOH]_n$ showing the corrugated topology and the alignment of the ^{n}hexoxy (in (b)) or ^{n}decoxy (in (c)) chains parallel to the *b*-axis.

Fig. 3. 2D→2D parallel interpenetrated networks within one sheet (*bc*-plane) in $[Zn_2Cl_4(\mathbf{4})]_n$ viewed (a) down the *a*-axis and (b) down the *c*-axis.
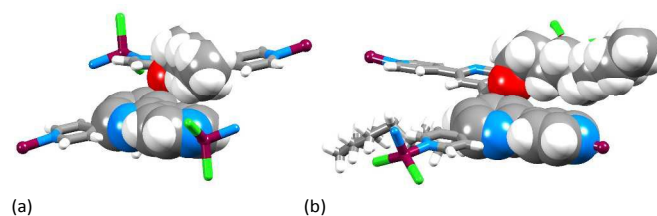

Fig. 4. Orientation of an (a) ^{n}hexoxy and (b) ^{n}decoxy chain over a 4,2':6',4''-tpy domain in $[Zn_2Cl_4(\mathbf{4})]_n$ and $[Zn_2Cl_4(\mathbf{5})\cdot 2MeOH]_n$, respectively.

The X-ray powder diffraction pattern of the bulk sample of $[Zn_2Cl_4(\mathbf{5})\cdot 2MeOH]_n$ (Fig. S1†) gave a reasonable fit with that predicted from the single crystal structure data. Shifts between observed and predicted peaks are expected since the powder and single crystal measurements were carried out at room temperature and 123 K, respectively. Crystals of $[Zn_2Cl_4(\mathbf{4})]_n$ readily lost solvent and this, combined with the use of SQUEEZE for $[Zn_2Cl_4(\mathbf{4})]_n$, resulted in a poor fit between the bulk sample powder diffraction pattern and that predicted from the single crystal structure.

Introduction of a terminal phenyl functionality

The consistency of structural architecture obtained for alkoxy tails containing between six and ten carbon atoms led us to consider the effects of introducing a structural unit to switch the assembly process. We have already shown that loss of long alkoxy functionalities results in retention of a (4,4) network but loss of 2D→2D parallel interpenetration.[14] We chose to replace the ^{n}alkoxy unit by a 3-phenylpropoxy substituent, retaining a length similar to ^{n}hexoxy but incorporating a terminal phenyl group. This terminal unit has potential for additional π-stacking interactions. Methanol solutions of $ZnCl_2$ or $ZnBr_2$ were each layered over a $CHCl_3$ solution of **6** but X-ray quality crystals grew only from the $ZnBr_2$ containing reaction mixture. Structural analysis revealed the formation of solvated $[Zn_2Br_4(\mathbf{6})\cdot H_2O]_n$. The solvent region in the structure proved problematical during refinement (see Experimental section), and crystals readily lost solvent resulting in a poor fit between

the bulk sample powder diffraction pattern and that predicted from the single crystal structure.

$[Zn_2Br_4(\textbf{6})·H_2O]_n$ crystallizes in the trigonal $R–3$ space group and the asymmetric unit contains one $ZnBr_2$ unit and half a molecule of **6**. The second half is generated by inversion and the repeat unit in $[Zn_2Br_4(\textbf{6})·H_2O]_n$ with symmetry generated atoms is shown in Fig. 5. The repeat unit resembles those in $[Zn_2Cl_4(\textbf{4})]_n$ (Fig. 1) and $[Zn_2Cl_4(\textbf{5})·2MeOH]_n$ (Fig. S6†). Bond angles in the coordination sphere of tetrahedral Zn1 are in the range 104.90 to 126.32(4)°, and bond distances (caption to Fig. 5) are unexceptional. The angles between the planes of the pyridine rings containing N1/N2 and N2/N3 are 22.0 and 12.5°, respectively, while the ring containing C16 is twisted through 51.4° with respect to the pyridine ring to which it is bonded.
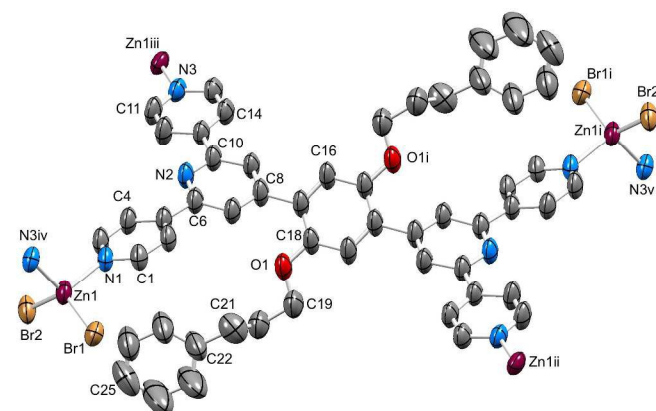

Fig. 5. The repeat unit (with symmetry generated atoms) in $[Zn_2Br_4(\textbf{6})·H_2O]_n$ (H atoms and water molecule omitted; ellipsoids plotted at 40% probability level). Symmetry codes: i = 1–x, 1–y, 2–z; ii = $^1/_3$–x+y, $^2/_3$–x, $^2/_3$+z; iii = $^2/_3$+x+y, $^1/_3$+x, $^4/_3$–z; iv = $-^1/_3$+y, $^1/_3$–x+y, $^4/_3$–z; v = $^4/_3$–y, $^2/_3$+x–y, $^2/_3$+z. Selected bond parameters: Zn1–N3^{iv} = 2.052(4), Zn1–Br1 = 2.3635(8), Zn1–Br2 =2.3462(8), Zn1–N1 = 2.058(3), O1–C18 = 1.382(6), O1–C19 = 1.435(8) Å; N3^{iv}–Zn1–Br1 = 104.90(11), N3^{iv}–Zn1–Br2 = 106.83(10), Br1–Zn1–Br2 = 126.32(4), N3^{iv}–Zn1–N1 = 105.99(15), Br1–Zn1–N1 = 105.36(11), Br2–Zn1–N1 = 105.97(11), C18–O1–C19 = 119.4(4)°.

As in $[Zn_2Cl_4(\textbf{4})]_n$ and $[Zn_2Cl_4(\textbf{5})·2MeOH]_n$, the bis(4,2':6',4''-tpy) ligand in $[Zn_2Br_4(\textbf{6})·H_2O]_n$ acts as a 4-connecting node and the Zn atom is a linker. However, in contrast to the 2D (4,4) nets in $[Zn_2Cl_4(\textbf{4})]_n$ and $[Zn_2Cl_4(\textbf{5})·2MeOH]_n$, the combination of $ZnBr_2$ and **6** leads to a 3D architecture. Fig. 6 shows an overlay of the repeat units of $[Zn_2Cl_4(\textbf{4})]_n$ and $[Zn_2Br_4(\textbf{6})·H_2O]_n$. The only significant difference between the two motifs is the direction in which the peripheral N donors (atoms N3iv and N3v in Fig. 1 and 5) point. This change is brought about by rotation about the Zn–N bonds and appears to be associated with the proximity of the terminal phenyl substituent to the $\{ZnX_2N_2\}$ unit. Unfortunately, we were not able to grow X-ray quality crystals of the chlorido-analogue of $[Zn_2Br_4(\textbf{6})·H_2O]_n$, but we propose that it is the presence of the phenyl group (rather than the bromine atoms) that directs the switch from 2D to 3D assembly. This conjecture is based upon the analogous 2D assemblies observed for $[\{Zn_2Cl_4(\textbf{2})\}·4H_2O]_n$ and $[\{Zn_2Br_4(\textbf{2})\}]_n$ (Table S1†).
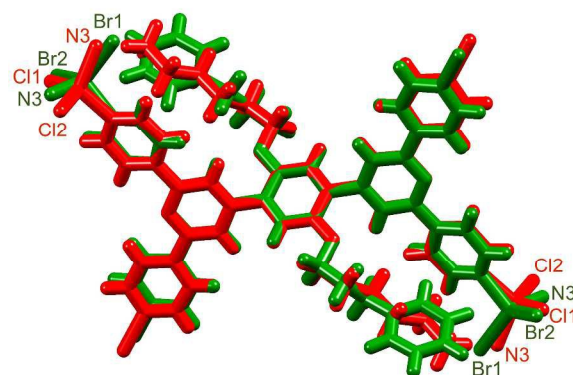

Fig. 6. Overlay of the repeat units with symmetry generated atoms of $[Zn_2Cl_4(\textbf{4})]_n$ (in red) and $[Zn_2Br_4(\textbf{6})·H_2O]_n$ (in green).

The structure of $[Zn_2Br_4(\textbf{6})·H_2O]_n$ propagates into a 3D-framework of 2-fold interpenetrating $\{6^4.8^2\}$ **nbo** nets.[26,27] Fig. 7 shows a TOPOS[23] representation of part of the lattice. The distortion away from an ideal **nbo** net arises from the difference between an archetype square-planar geometry and the X-shaped 4-connecting node of **6** which has internal angles of 54.3 and 125.7°. The $R–3$ symmetry leads to hexagonal channels which follow the crystallographic c-axis (Fig. 8 and S8†). As Fig. 8a shows, the pendant phenyl rings are directed into the channels and each ring is oriented to face a 4,2':6',4''-tpy in the adjacent net. The distance between the centroid of the phenyl ring with C22 and the least squares plane through the two pyridine rings containing N2^{vi} and N3^{vi} (symmetry code vi = $^1/_3$+x–y, $-^1/_3$+x, $^5/_3$–z) is 3.57 Å, and the angle between the planes through these units is 7.1°. The shortest distance between a C_{phenyl} atom (C27) and the centroid of the unit comprising the two pyridine rings with N2^{vi} and N3^{vi} is 3.77 Å. The relative positions of the two aromatic units is too far offset for the interaction to be classed as a typical face-to-face π-stacking contact.[28,29] Nonetheless, the interactions around the walls of the hexagonal channels serve to lock the interpenetrated nets in close proximity to one another, leaving large voids in the lattice. The solvent accessible void space in the lattice represents ~65% of the total volume[21] (Fig. 8b). The close association of two interpenetrated **nbo** nets leading to large, unobstructed channels has also been described by Hawes *et al.*,[30] and Chun and coworkers[31] in related structures that crystallize in the $R–3$ space group. Both these assemblies are predicated upon copper(II) 4-connecting nodes and organic linkers. In the first example,[30] the **nbo** nets associate through NH...O hydrogen bonded interactions. In the second,[31] non-coordinated N-donors of pyrimidine-5-carboxylate linkers in one **nbo** net weakly bind to square planar copper(II) nodes in the second net. Interestingly, attempts to produce a corresponding assembly by replacing pyrimidine-5-carboxylate by pyridine-3-carboxylate linkers (thereby removing the additional N-donors) were unsuccessful.[31] This lends support to our premise that the peripheral phenyl groups in **6** play a role in stabilizing the interpenetrated 3D architecture in $[Zn_2Br_4(\textbf{6})·H_2O]_n$. A number of related assemblies (space group $R–3$) involving 2-fold interpenetrating **nbo** nets with

large-diameter hexagonal channels running parallel to the *c*-axis have been described.[32] In each case, the 4-connecting nodes are metal ions and the linkers are organic ligands. This contrasts with the reverse situation in $[Zn_2Br_4(\mathbf{6})\cdot H_2O]_n$.
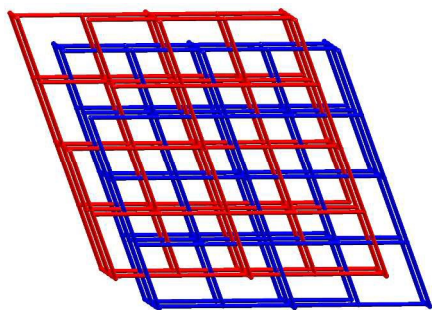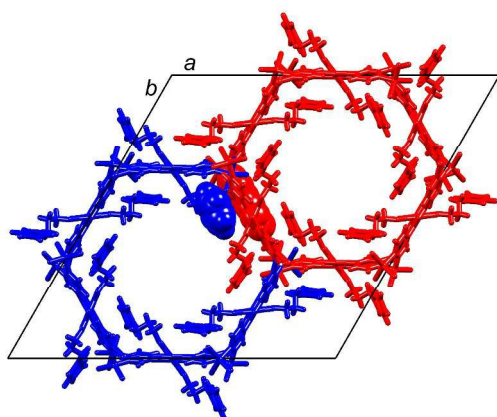

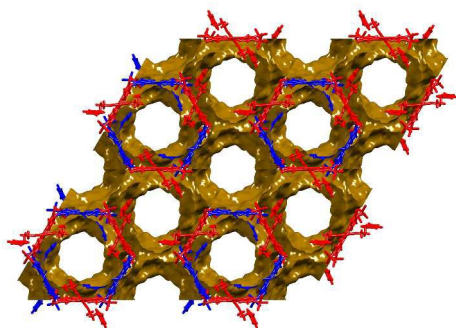**Fig. 7.** TOPOS[23] representation of the interpenetrated **nbo** nets in $[Zn_2Br_4(\mathbf{6})\cdot H_2O]_n$.

(a)

(b)

Fig. 8. (a) Parts of interpenetrated nets (red and blue) in $[Zn_2Br_4(\mathbf{6})\cdot H_2O]_n$. View down the *c*-axis showing location of the terminal phenyl groups within the hexagonal channels; one stacking contact is shown in space-filling representation. (b) View down the *c*-axis showing the void space in the hexagonal channels (drawn using Mercury v. 3.7[21,22]).

Conclusions

We have described the synthesis and characterization of three ditopic bis(4,2':6',4''-tpy) ligands, **4–6**. Ligands **4** and **5** bear [n]hexoxy and [n]decoxy tails, respectively, while **6** is functionalized with 3-phenylpropoxy tails. Reactions of **4** or **5**

with $ZnCl_2$ lead to $[Zn_2Cl_4(\mathbf{4})]_n$ or $[Zn_2Cl_4(\mathbf{5})\cdot 2MeOH]_n$, respectively. The compounds crystallize in the *C*2/*c* space group with similar 2D→2D parallel interpenetrating (4,4) nets; the ditopic ligands act as planar 4-connecting nodes. The [n]alkoxy tails are in extended conformations and are threaded within the sheets. The close structural similarities between $[Zn_2Cl_4(\mathbf{4})]_n$ and $[Zn_2Cl_4(\mathbf{5})\cdot 2MeOH]_n$ and the previously reported $[\{Zn_2Cl_4(\mathbf{2})\}\cdot 4H_2O]_n$ and $[\{Zn_2Br_4(\mathbf{2})\}]_n$[13,14] provide strong support for the network being invariant for [n]alkoxy tails containing six to ten carbon atoms. However, the presence of [n]alkoxy tails is a prerequisite for the 2D→2D parallel interpenetration. The introduction of a terminal phenyl group in going to ligand **6** switches the 2D assembly to a highly porous 3D architecture. $[Zn_2Br_4(\mathbf{6})\cdot H_2O]_n$ crystallizes in the *R*–3 space group and the structure comprises 2-fold interpenetrating **nbo** nets. Again, the 4-connecting nodes are the bis(4,2':6',4''-tpy) ligands, contrasting with related structures in which the 4-connecting nodes are metal centres.[30,31,32] The pendant phenyl rings in **6** lie over the 4,2':6',4''-tpy domains in an adjacent net and these contacts result in tight interlocking of the interpenetrated nets. As a consequence of this, the lattice contains hexagonal channels which follow the crystallographic *c*-axis. We are now exploring the consequences of adapting the terminal functionality, in an effort to better understand[33,34] the factors that direct the interpenetration of the 3D-nets.

Notes and references

[a]Department of Chemistry, University of Basel, Spitalstrasse 51, CH-4056 Basel, Switzerland; email: catherine.housecroft@unibas.ch

†Electronic Supplementary Information (ESI) available: Table S1: Comparison of cell parameters for related compounds; Fig. S1: Powder diffraction data; Fig. S2-S5: ^{1}H NMR spectra of compounds **4-6**; Fig. S6-S8: Additional structural diagrams. CCDC 1541159-1541161. See DOI: 10.1039/b000000x/

1 C. E. Housecroft, *Dalton Trans.*, 2014, **43**, 6594.

2 C. E. Housecroft, *CrystEngComm*, 2015, **17**, 7461.

3 See for example: S. Khatua, A.K. Bar and S. Konar, *Chem. Eur. J.*, 2016, **22**, 16277; S. Khatua, S. Goswani, S. Biswas, K. Tomar, H.S. Jena and S. Konar, *Chem. Mater.*, 2015, **27**, 5349; A.K. Mondal, S. Khatua, K. Tomar and S. Konar, *Eur. J. Inorg. Chem.*, 2016, 3545; Y.M. Klein, A. Prescimone, E.C. Constable and C.E. Housecroft, *Aus. J. Chem.* 2017, doi.org/10.1071/CH16527; M. Zhao, J. Tan, J. Su, J. Zhang, S. Zhang, J. Wu and Y. Tian, *Dyes Pigments*, 2016, **130**, 216; G. Zhang, J. Tan, T. Phoenix, D.R. Manke, J.A. Golen and A.L. Rheingold, *RSC Adv.*, 2016, **6**, 9270; Z. Yin, S. Zhang, S. Zheng, J. A. Golen, A. L. Rheingold and G. Zhang, *Polyhedron*, 2015, **101**, 139; L. Li, Y.Z. Zhang, C. Yang, E. Liu, J.A. Golen and G. Zhang, *Polyhedron*, 2016, **105**, 115; Y.M. Klein, A. Prescimone, E.C. Constable and C.E. Housecroft, *Polyhedron*, 2016, **103A**, 58; Y.M. Klein, A. Prescimone, M.B. Pitak, S.J. Coles, E.C. Constable, C.E. Housecroft, *CrystEngComm*, 2016, **18**, 4704 and references therein.

4 F. Kröhnke, Synthesis, 1976, 1.

5 J. Wang and G.S. Hanan, *Synlett*, 2005, 1251.

6 See for example: M. Lusi, P.B.A. Fechine, K.-J. Chen, J.J. Perry IV and M.J. Zaworotko. *Chem. Commun.*, 2016, **525**, 4160; N. Li and R. Huang, *J. Solid State chem.*, 2016, **233**, 320; W. Sun, J. Liu, H. Liu and Z. Liu, *Polyhedron*, 2016, **109**, 1.

7 See for example: Y. Wu, L. Lu, J. Feng, Y. Li, Y. Sun, A. Ma, *J. Solid State Chem.*, 2017, **245**, 213; Z.-L. Wu, C.-H. Wang, B. Zhao, J. Dong, F. Lu, W.-H. Wang, W.-C. Wang, G.-J. Wu, J.-Z. Cui and P. Cheng, *Angew. Chem. Int. Ed.*, 2016, **55**, 4938; X. Li, X.-L. Chi, Y.-C. Xu, Y. Chen, Q. Yang, X.-S. Zeng, H.-L. Xu and D.-R. Xiao, *Inorg. Chem. Comm.*, 2016, **69**, 52; J. Liu, J. Xiao, D. Wang, W. Sun, X. Guo, H. Yu, H. Liu and Z. Liu, *Cryst. Growth Des.*, 2016, **17**, 1096;

8 Y. Watanabe, R. Yoshioka, H. Sasabe, T. Kamata, H. Katagiri, D. Yokoyama, J. Kido, *J. Mater. Chem. C*, 2016, **4**, 8980.

9 J. Lü, C. Perez-Krap, M. Suyetin, N. H. Alsmail, Y. Yan, S. Yang, W. Lewis, E. Bichoutskaia, C. C. Tang, A. J. Blake, R. Cao and M. Schröder, *J. Am. Chem. Soc.*, 2014, **136**, 12828.

10 Y.M. Klein, A. Prescimone, E.C. Constable and C. E. Housecroft, *Inorg. Chem. Comm.*, 2016, **70**, 118.

11 J. Yoshida, S.-I. Nishikiori and H. Yuge, *J. Coord. Chem.*, 2013, **66**, 2191.

12 Y.M. Klein, E.C. Constable, C.E. Housecroft and A. Prescimone, *CrystEngComm*, 2015, **17**, 2070.

13 E.C. Constable, C.E. Housecroft, S. Vujovic and J.A. Zampese, *CrystEngComm,* 2014, **16**, 3494; E.C. Constable, C.E. Housecroft, S. Vujovic and J.A. Zampese, *CrystEngComm,* 2017, DOI: 10.1039/c7ce90062g.

14 S. Vujovic, E.C. Constable, C.E. Housecroft, C.D. Morris, M. Neuburger and A. Prescimone, *Polyhedron*, 2015, **92**, 77.

15 C.L. Moy, R. Kaliappan and A.J. McNeil, *J. Org. Chem.*, 2011, **76**, 8501.

16 M.K. Choi, H.L. Kim, D.H. Suh, *J. Appl. Polym. Sci.,* 2006, **101**, 1228.

17 Stoe & Cie (2011). X-area Software, Stoe & Cie (1996). XRED V1.08.

18 L. Palatinus and G. Chapuis, *J. Appl. Cryst.*, 2007, **40**, 786.

19 P.W. Betteridge, J.R. Carruthers, R.I. Cooper, K. Prout and D.J. Watkin, *J. Appl. Cryst.*, 2003, **36**, 1487.

20 A.L. Spek, *Acta Crystallogr., Sect. C*, 2015, **71**, 9.

21 I. J. Bruno, J. C. Cole, P. R. Edgington, M. K. Kessler, C. F. Macrae, P. McCabe, J. Pearson and R. Taylor, *Acta Cryst.*, 2002, **B58**, 389.

22 C.F. Macrae, I.J. Bruno, J.A. Chisholm, P.R. Edgington, P. McCabe, E. Pidcock, L. Rodriguez-Monge, R. Taylor, J. van de Streek and P. A. Wood, *J. Appl. Cryst.*, 2008, **41**, 466.

23 V. A. Blatov, A. P. Shevchenko, TOPOS Professional v. 4.0, Samara State University, Russia.

24 M. Nishio, *CrystEngComm*, 2004, **6**, 130.

25 C.R. Groom, I.J. Bruno, M.P. Lightfoot and S.C. Ward, *Acta Cryst.*, 2016, **B72**, 171.

26 D.-S. Li, Y.-P. Wu, J. Zhao, J. Zhang and J.Y. Lu, *Coord. Chem. Rev.*, 2014, **261**, 1.

27 S.R. Batten, S.M. Neville and D.R. Turner, *Coordination Polymers: Design, Analysis and Application*, RSC Publishing, Cambridge, 2009.

28 C.A. Hunter and J.K.M. Sanders, *J. Am. Chem. Soc.*, 1990, **112**, 5525.

29 C.A. Hunter, K.R. Lawson, J. Perkins and C.J. Urch, *J. Chem. Soc., Perkin Trans. 2*, 2001, 651.

30 C.S. Hawes, R. Babarao, M.R. Hill, K.F. White, B.F. Abrahams and P.E. Kruger, *Chem. Commun.*, 2012, **48**, 11558.

31 J. Seo, N. Jin and H. Chun, *Inorg. Chem.*, 2010, **49**, 10833.

32 See for example: W.-W. Dong, L. Xia, Z. Peng, J. Zhao, Y.-P. Wu, J. Zhang, D.-S. Li, *J. Solid State Chem.*, 2016, **238**, 170; P. Yang, H.-Y. Zhou, K. Zhang and B.-H. Ye, *CrystEngComm*, 2011, **13**, 5658; G.-G. Hou, Y. Liu, Q.-K. Liu, J.-P. Ma and Y.-B. Dong, *Chem. Commun.*, 2011, **47**, 10731; D. Liu, M. Li and D. Li, *Chem. Commun.*, 2009, 6943.

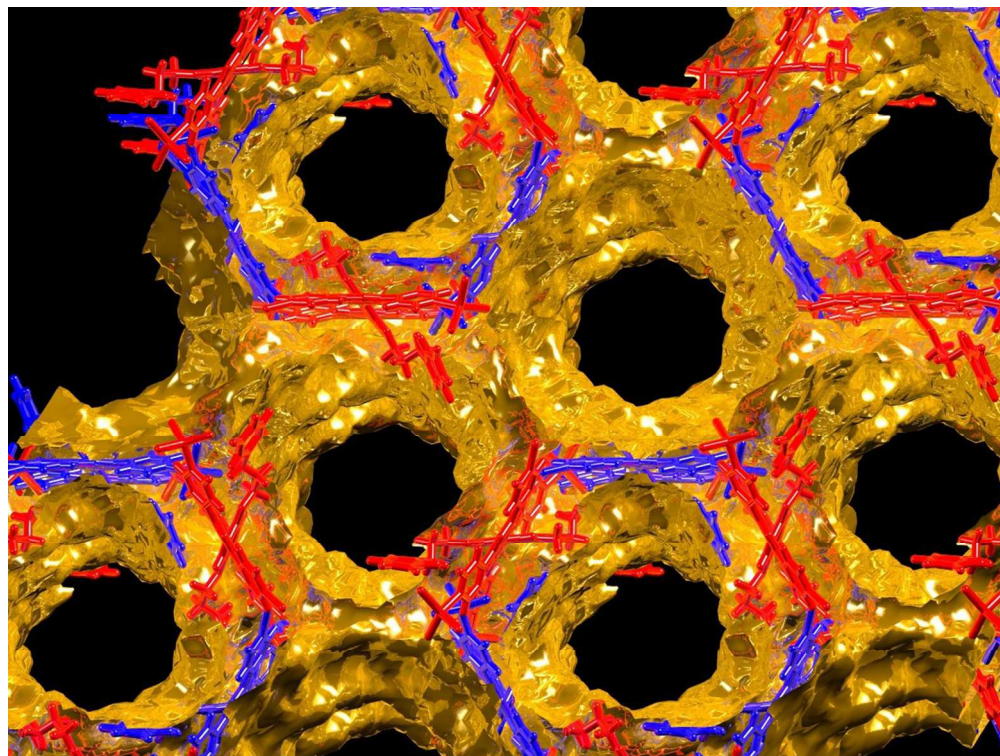33 S.R. Batten, *J. Solid State Chem.*, 2005, **178**, 2475.

34 D. Zhao, D.J. Timmons, D. Yuan and H.-C. Zhou, *Acc. Chem. Res.*, 2011, **44**, 123.

TOC

What a difference a tail makes: 2D→2D parallel interpenetration of sheets to interpenetrated nbo networks using ditopic-4,2':6',4''-terpyridine ligands

Y.M. Klein, A. Prescimone, M. Neuburger, E.C. Constable and C.E. Housecroft*

When 1,4-bis(n-alkoxy)-2,5-bis(4,2':6',4''-terpyridin-4'-yl)benzenes react with

ZnX_2 (X = Cl, Br), the presence of terminal phenyl groups causes a switch from

2D→2D parallel interpenetrated nets to 2-fold interpenetrating **nbo** nets.

451x338mm (72 x 72 DPI)